# A Beam Window Target Design with Independent Cooling for the EADF

C. Aragonese, S. Buono, G. Fotia, L. Maciocco, V. Moreau, L. Sorrentino

(30 November, 2000)

## Introduction

This report summarizes the study and the design of the window type target for the Energy Amplifier Demonstration Facility (EADF) [1]. The behaviour of the system in different condition has been analysed though extensive CFD simulations performed with the Star-CD commercial code [2].
The target represents one of the main technological problems related not only to the design of the EADF, but to all High Power Spallation Sources (HPSS) currently under study or in construction world-wide [4],[5].
Different configurations of the spallation EADF target are possible. Advantages and disadvantages of the different options are discussed elsewhere [6] and they are studied and analysed separately.
The target device studied in this report is a window type target, cooled by diathermic oil in an independent loop. This target configuration is completely independent from the core operating conditions and gives advantages in terms of flexibility in the operation.
The result of this report is a set of design data and constraints to take into account while engineering the spallation target.

## Target Geometry

The target geometry, illustrated in figure 1, is of axial-symmetric type and is constituted of a vertical pipe closed at the bottom by the beam window. The beam pipe is embedded in a coaxial container. The container is insulated in order to minimise heat exchanges with the primary cooling loop Lead Bismuth Eutectic (LBE).
The space between the beam pipe and the container is occupied by the spallation material (LBE) which acts as a coolant too. Inside the beam pipe a, high vacuum is mantained.
The coolant flow, driven by natural convection forces, is guided by a flow guide laying between the beam pipe and the container. It separates the hot rising flow coming from the spallation region from the cold down coming flow cooled in the heat exchanger, which is located at the top of the downcomer channel.
In the spallation zone the flow guide is shaped like a funnel in order to enhance the cooling of the window and the spallation region. The funnel is made of a converging duct, which reverses the flow from the downcomer channel into a narrow pipe where the spallation take place. The funnel and the hot fluid rising channel are connected by a divergent.

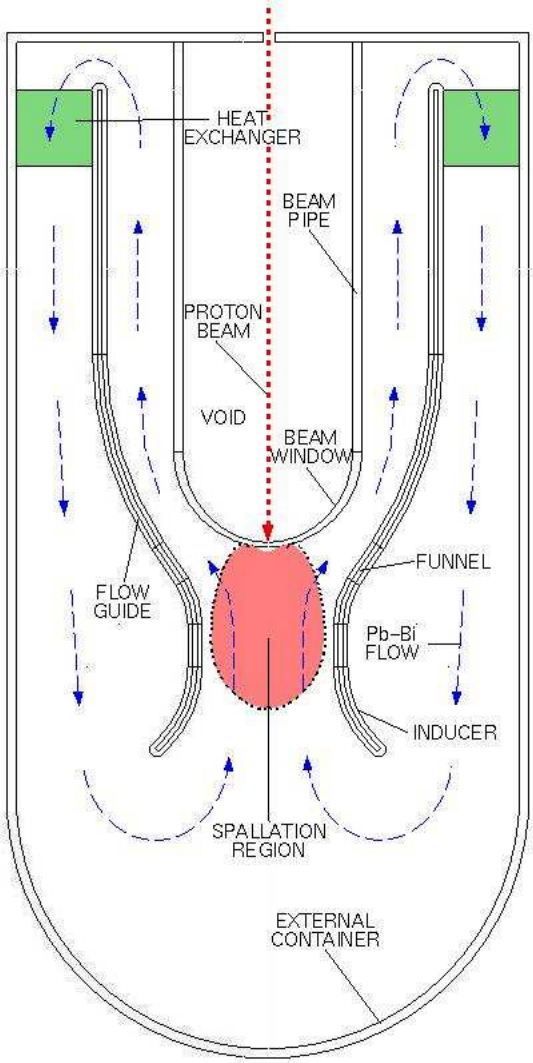


**Figure 1: Target device scheme**

The main geometrical data are reported in .

| symbol | Description | value |
|---|---|---|
| $H_{tot}$ | Target height | 7 m |
| $D_c$ | Container diameter | 544 mm |
| $D_{fg}$ | flow guide diameter | 340 mm |
| $D_p$ | beam pipe diameter | 200 mm |
| $L_f$ | Funnel length | 300 mm |
| $D_f$ | Funnel diameter | 140 mm |
| $H_{he}$ | Heat exchanger height | 2 m |
| $H_{riser}$ | Riser height | 5.9 m |

**Table 1: window type target main geometrical data**

The geometric parameters of the target model are illustrated in Figure 2. Table 2 shows the values of these parameters.

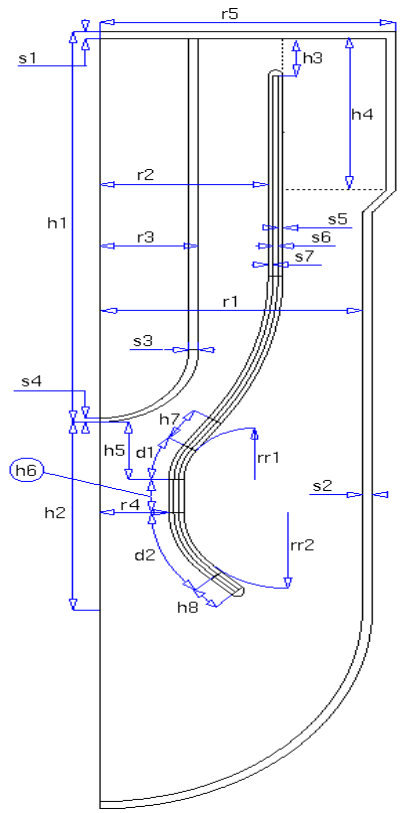


**Figure 2: Geometric parameter of the target unit**

| Parameter | [mm] | parameter | [deg] | parameter | [mm] | parameter | [mm] |
|---|---|---|---|---|---|---|---|
| r1 | 275 | d1 | 34 | s1 | 3.0 | h1 | 6400 |
| r2 | 170 | d2 | 45 | s2 | 3.0 | h2 | 550 |
| r3 | 100 | | | s3 | 3.0 | h3 | 200 |
| r4 | 70.0 | | | s4 | 1.0 | h4 | 1500 |
| r5 | 300 | | | s5 | 1.3 | h5 | 80 |
| rr1 | 71.5 | | | s6 | 1.4 | h6 | 150 |
| rr2 | 100 | | | s7 | 1.3 | h7 | 45.5 |
| | | | | | | h8 | 10 |

**Table 2: values of target geometrical parameters**

## Physical Properties

The structural materials to be used in the target device must be able to work properly in severe condition. The main requirements are essentially:

**1** Capability of sustaining conventional loads such as temperature and mechanical stresses. Such loads can be quite high.

**2** Compatibility with the radiation environment: materials are exposed to a neutron flux which is at least equal in intensity and harder in spectrum than the one experienced by the closest pins of the EADF core.

**3** Compatibility with a high-energy proton flux.

**4** Compatibility with liquid metal environment (LBE)

The choice of the beam window material is therefore very delicate and depends on many factors (physical and structural properties, activation properties, working temperature, and compatibility with liquid Pb-Bi environment) which are often not independent one on another.

The material chosen, according to [7] and [8], is a Low Activation Martensitic Steel (LAMS) and in particular the 9Cr 1Mo V Nb steel. The materials properties are considered as function of the temperature and the relationships used are reported in Table 3

| Property | Lead Bismuth Eutectic | 9Cr 1Mo V Nb steel | | |
|---|---|---|---|---|
| Density [kg/m$^3$] | 11112.38 - 1.37 T | 7847.21 - 0.35 T | | |
| Thermal conductivity [W/ m K] | 3.029214 $10^{-5}$ $T^2$ - 1.831813 $10^{-2}$ T +11.48094 | -6.323541 $10^{-6}$ $T^2$ + 1.441486 $10^{-2}$ T +22.23979 | | |
| Specific heat [J / kg K] | 146.5 | 3.811905 $10^{-4}$ $T^2$ + 6.405714 $10^{-3}$ T +433.8646 | | |
| Molecular viscosity [Pa s] | 4.713675 $10^{-9}$ $T^2$ - 8.9224 $10^{-6}$ T + 5.371479 $10^{-3}$ | | | |
| | | 200 °C | 300 °C | 400 °C |
| Young modulus [MPa] | | 207 | 199 | 190 |
| Poisson ratio | | 0.29 | 0.29 | 0.29 |
| Thermal expansion coeff. [$10^{-6}$ /K] | | 11.3 | 11.7 | 12.0 |
| Yield strength [MPa] | | 500 | 495 | 480 |

**Table 3: Target material physical properties**

## Computational Model

### Numerical schemes

Due to geometrical symmetry consideration, only 1/72 of the target has been considered in the simulation, equivalent to an angle of 5 degrees out of 360. The simulation was performed in steady state conditions using the commercial code STAR-CD V.3.100. [2]. The numerical model employs a third order scheme ("QUICK") for the spatial discretisation of the convective terms and an upwind scheme ("UD") for $k$- $\varepsilon$.
When needed, for example for the simulation of start-ups, the analysis was done in transient conditions. In this case, the "PISO" algorithm was used. References of these algorithms can be found in the code methodology manual.

### Turbulence model

The Chem $k$-$\varepsilon$ model, coupled with a Norris&Reynolds two layer model for the simulation of low-Reynolds number effects in the near wall regions.

### Boundary conditions

The boundary conditions of the system are the following:

**1** the container is supposed adiabatic;
**2** oil inlet temperature (150 - 200 °C);
**3** oil mass flow rate (31.2 kg/s);
**4** proton beam heat deposition field
**5** beam pipe is supposed adiabatic;
**6** Two paired cyclic boundaries are applied on the lateral surface of the sector.

### Computational Grid

The IDEAS CAD and mesh generator have been used to create a parametric mixed structured-unstructured mesh. Unstructured meshes are used in zones with irregular geometry and whose shape was optimised, like the funnel zone as shown in Figure 3. The fluid regions near the walls are meshed with structured grids, easier to handle and more suitable for the application of the turbulent near-wall algorithms.

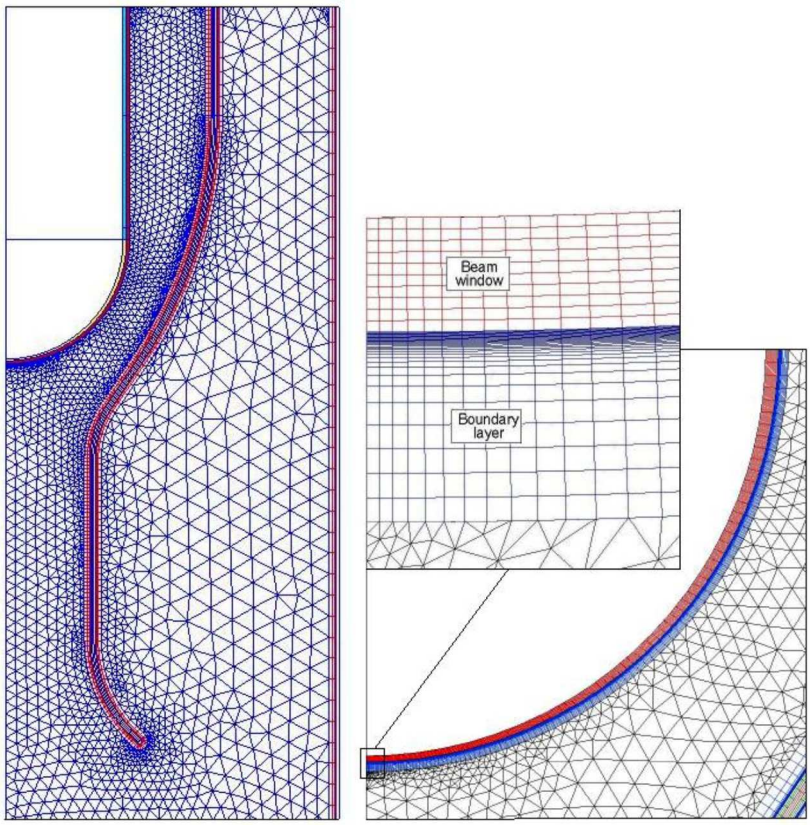


**Figure 3: The non-structured mesh in the funnel zone and the structured mesh in the window and in the near-wall region.**

Structured meshes are also used for the discretization of the solids. In order to make possible the use of meshes with different coarseness in the rising and downcoming sides, the flow guide is discretized with a non-conform mesh.
The total number of cells is about 25000. The discretization is very accurate in the funnel zone, especially close to the window stagnation point. Cells with high aspect ratio are used in the rising and downcoming duct, where the flow is supposed to be regular.

## Spallation Heat Source

The interactions between the proton beam and the window and coolant materials are simulated with the FLUKA code [9]. The result of this calculation, a Montecarlo simulation using 1.000.000 protons, is the volumetric heat source distribution showed in figure 5 as it is given as input to the CFD simulation.
The heat source distribution in the window is given by an analytical curve as a function of the distance from the beam axis. The curves for the 9Cr 1Mo V Nb steel window exposed to a 150 mm diameter proton beam with an energy of 600 MeV and a parabolic intensity distribution are given below:

for $0 < r < 75$ mm  $q = -1.020457\, r^2 + 4.124325\, r + 27.42338$  [W/cm$^3$ mA]
for $75 < r < 100$ mm  $q = -0.3341885\, r + 3.983076$  [W/cm$^3$ mA]

where r is the distance from the beam axis (in cm).

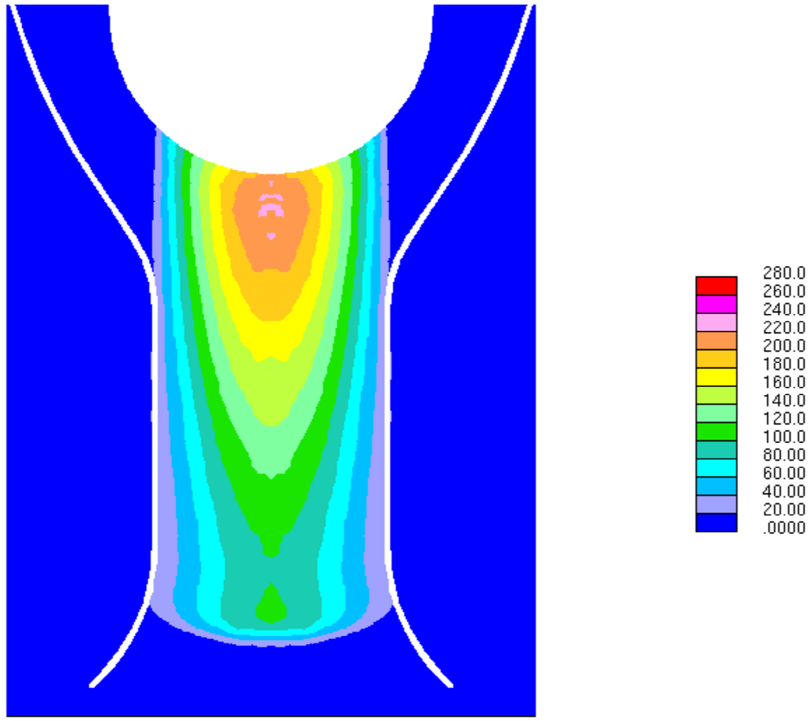


**Figure 4 FLUKA heat source distribution in the Pb-Bi eutectic [W/cm$^3$ mA]**

## Heat Exchanger

A bayonet-type heat exchanger (BHE) for the target has been designed [10]. The scheme for a single tube is reported in Figure 5. The main requirement was to keep length and pressure drops as low as possible, in order to allow the use of natural circulation for the cooling of the target in standard operating conditions. In this case, the use of pumping methods as, for example, gas injection could be limited to start-up and accidental events or even suppressed at all.

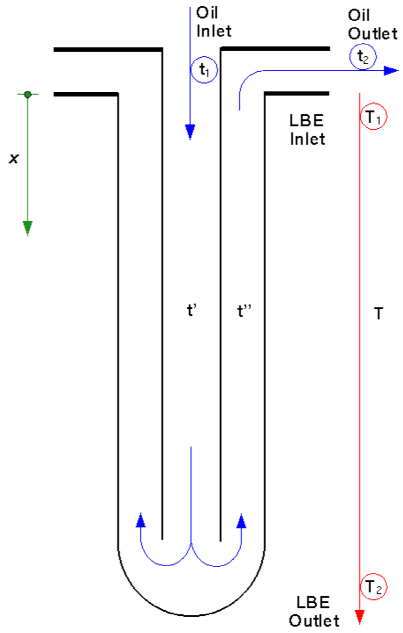


**Figure 5: Bayonet heat exchanger single tube scheme**

Different BHE configurations were considered for the heat load (2.6 MW) corresponding to the maximum target power at 6 mA:

BHE1: Dc = 550 mm, mfr = 250 kg/s, L = 2.0 m, Pd = 3870 Pa;
BHE2: Dc = 550 mm, mfr = 200 kg/s, L = 1.7 m, Pd = 2320 Pa;
BHE3: Dc = 592 mm, mfr = 250 kg/s, L = 1.8 m, Pd = 2510 Pa;
BHE4: Dc = 592 mm, mfr = 200 kg/s, L = 1.5 m, Pd = 1510 Pa;

where Dc is the internal diameter of the target container, mfr the mass flow rate, L the BHE tubes length and Pd the pressure drop.

A realistic model of the heat exchanger was then implemented in the target CFD simulation, taking into account the correlations for heat transfer and pressure loss coefficients. In the HE CFD model both LBE and oil side of the bayonet heat exchanger were considered, obtaining a detailed simulation of the local heat transfer.
Overall heat transfer and friction factor expression where used and applied locally to the single cells of the grid. This is possible since our computational cells contains different tubes and can be considered as a little heat exchanger.
The relations used for heat transfer and pressure drops calculation [10] are the following:

| Quantity | Relationship | Comments |
|---|---|---|
| Nusselt oil internal pipe | $0.023\ Re^{0.8}\ Pr^{0.333}$ | Sieder-Tade eqs. for tubes |
| Nusselt oil annuli | $0.02\ Re^{0.8}\ Pr^{0.333}\ (d_e/D_i)^{0.53}$ | Monrad and Pelton equation. for annuli |
| Nusselt LBE longitudinal | $7 + 0.025\ Re^{0.8}\ Pr^{0.8}$ | Martinelli equation for liquid metals |
| Nusselt LBE transversal | $4.03 + 0.0228\ (Re_{max}Pr)^{0.67}$ | Brookhaven Laboratory |

| | | |
|---|---|---|
| | | equation for liquid metals |
| Friction factor oil internal pipe | $0.079\ Re^{-0.25}$ | |
| Friction factor annuli | $0.087\ Re^{-0.25}$ | |
| Friction factor LBE longitudinal | $0.079\ Re^{-0.25}$ | |
| Friction factor LBE transversal | $(0.0675+0.03186/R_f)\ Re^{-0.16}$ | $R_f=[(S_T-D_e)/D_e]^{1.08}$ |

The BHE1 configuration was considered as first step obtaining a computed mass flow rate of 195 kg/s demonstrating the feasibility of natural-circulation cooling for the window-type target.
In order to enhance this mass flow rate the upper part of the container was enlarged and the BHE4 option was considered. The main result was an higher LBE mass flow rate (227 kg/sec) and lower window temperatures.

## Structural Analysis

The same grid used for the CFD simulation was employed for the finite element structural calculation. The nodes belonging to the surface on the top of beam pipe have been constrained with a slider that restrains the displacements normal to the plane of that surface. The choice of this constraint is not relevant because its effects are quickly damped in the very vicinity of the constraint itself. The temperature field calculated by Star-CD is assigned to the elements of the model and the Pb-Bi hydrostatic pressure distribution is applied onto the external surface.
Details of the procedure adopted can be found in [nea98, oecd99]. da inserire calcoli strutturali.

## Results and Discussion

Different target operating conditions were verified in the simulation as it is summarised in Table 4. The first simulation done was case d) which mainly demonstrates that natural convection cooling of the window is attainable.

In fact CFD calculations performed with the target configuration considered lead to the main result that the LBE flow can be driven only by natural convection, reaching velocities in the funnel zone high enough to ensure an appropriate heat removal rate.

The critical part is the funnel zone whose velocity field and velocity magnitude distribution is reported in Figure 6

Figure 7 shows the temperature distribution in the spallation zone, pointing out that, in spite of the high power involved, the temperatures reached are acceptable for the constitutive materials of the target. It can also be seen from Figure 8 where the temperature profile of the beam window is reported.

Another interesting part of the target is its top zone, where the LBE is reversed from the riser to the downcomer duct flowing across the bayonet heat exchanger. Figure 9 shows the temperature profile in this zone: on the left the LBE temperature is reported while on the right the heat exchanger grid is duplicated twice in order to show oil side temperature in the annulus and in the inner tube respectively

| Target option | **a)** | **b)** | **c)** | **d)** | |
|---|---|---|---|---|---|
| BHE bundle ext. diameter **(input data)** | 592 | 592 | 592 | 550 | mm |
| Window center thickness **(input data)** | 1.0 | 1.0 | 1.5 | 1.5 | mm |
| Energy of proton beam **(input data)** | 600 | 600 | 600 | 600 | MeV |
| Intensity of proton beam **(input data)** | 6 | 6 | 2-6 | 6 | mA |
| LBE mass flow rate | 227 | 226 | 226 | 195 | kg/s |
| Oil mass flow rate **(input data)** | 31.2 | 31.2 | 46.3 | 31.2 | kg/s |
| Mean LBE temp. in the riser | 325 | 276 | 268 | 272 | °C |
| Mean LBE temp. in the downcomer | 250 | 201 | 193 | 194 | °C |
| Maximum LBE temperature | 483 | 435 | 442 | 468 | °C |
| Maximum window temperature | 502 | 454 | 485 | 511 | °C |
| Max. window temp. radial gradient | 24 | 24 | 43 | 43 | °C |
| Mean LBE temp. in the HE inlet | 320 | 265 | 257 | 251 | °C |
| Mean LBE temp. in the HE outlet | 238 | 190 | 183 | 176 | °C |
| Oil temp. in the HE inlet **(input data)** | 200 | 150 | 150 | 150 | °C |
| Oil temp. in the HE outlet | 246 | 196 | 181 | 191 | °C |
| Mean LBE velocity in the riser | 0.372 | 0.368 | 0.367 | 0.318 | m/s |
| Mean LBE velocity in the downcomer | 0.159 | 0.157 | 0.157 | 0.136 | m/s |
| Maximum LBE velocity (in the funnel) | 1.52 | 1.51 | 1.50 | 1.29 | m/s |

**Table 4: Steady state operating condition for the target**

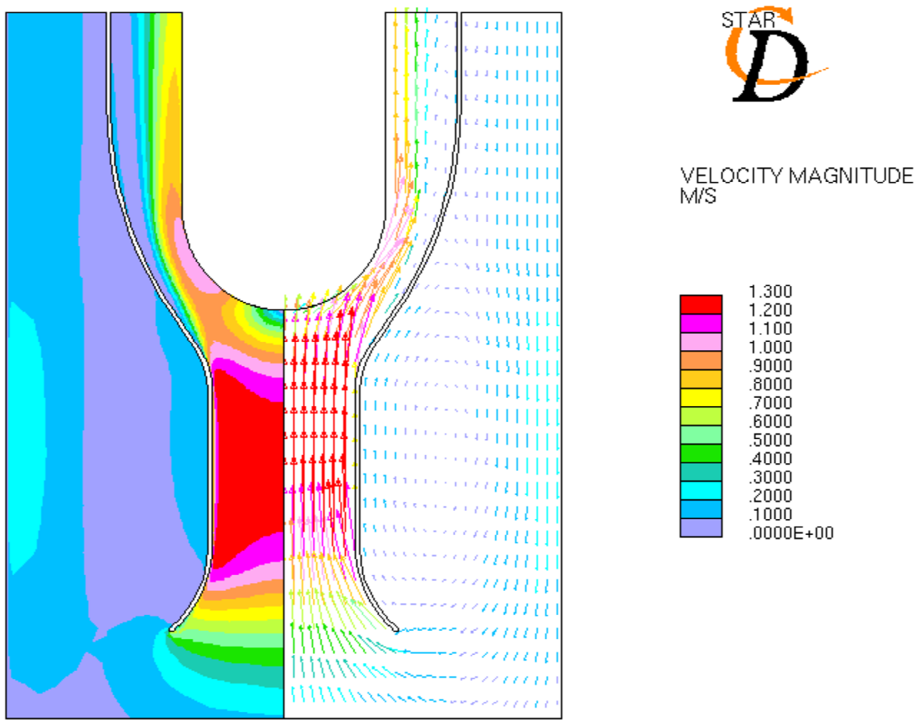


**Figure 6: case d) Velocity field and velocity magnitude distribution in the spallation zone of the target**

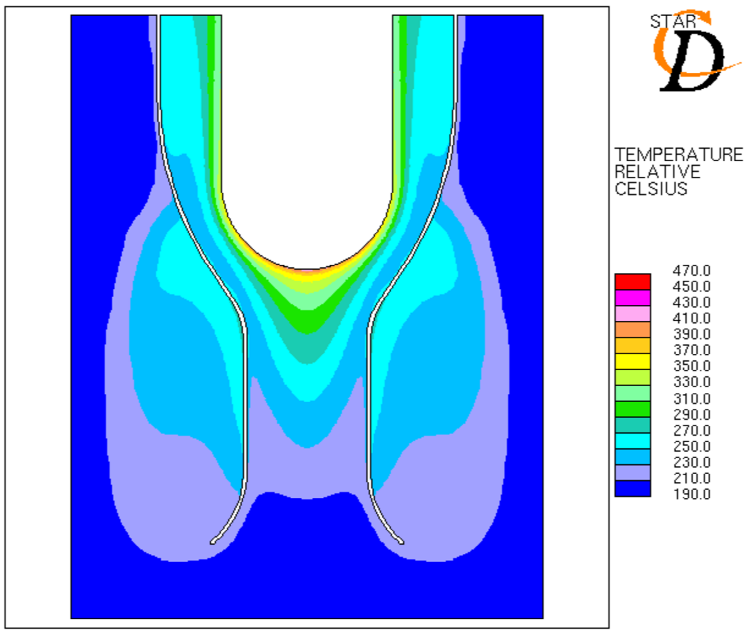


**Figure 7: case d) LBE temperature distribution in the spallation zone of the target**

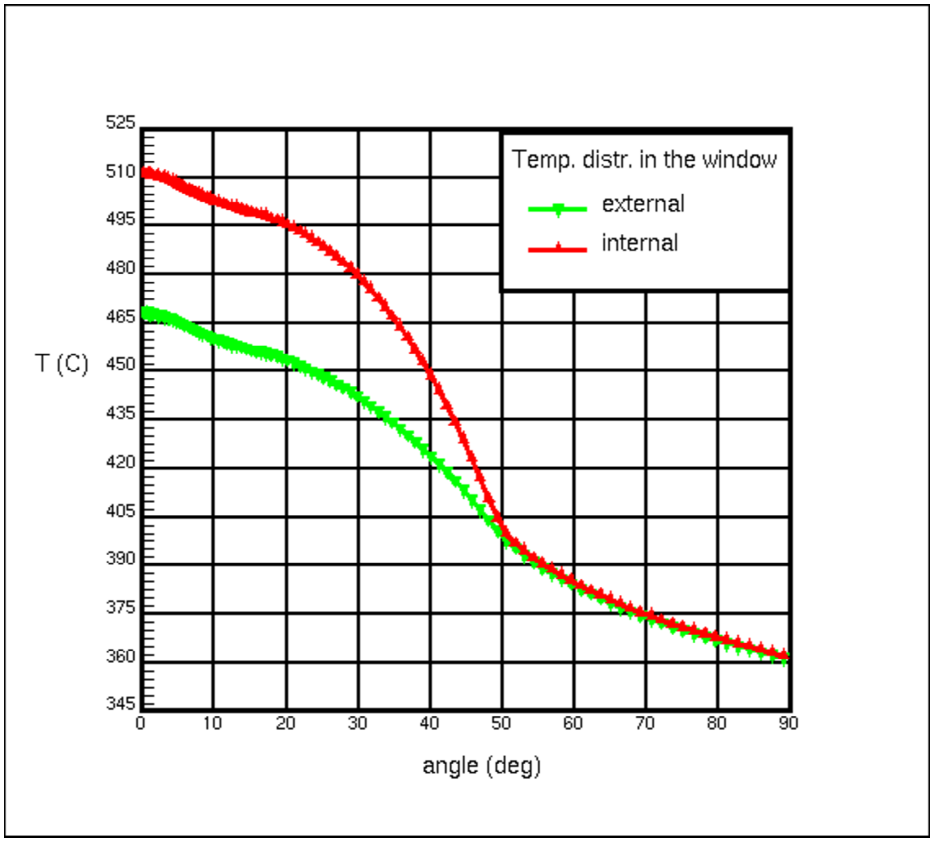


**Figure 8: case d) Beam window temperature profile in steady state conditions.**

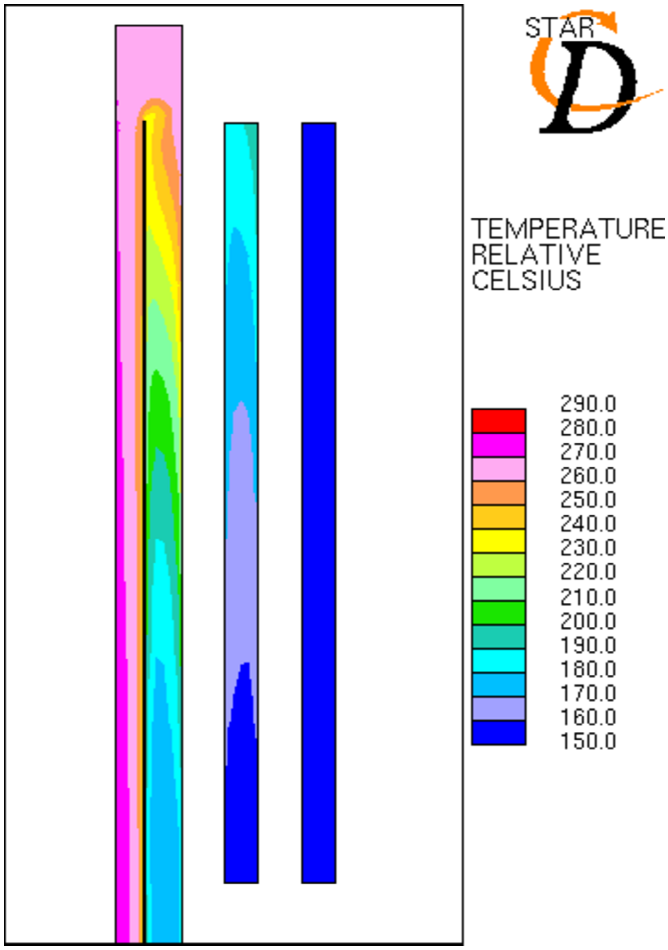


**Figure 9: case d) Temperature distribution in the top zone of the target and in the heat exchanger**

| | |
|---|---|
| Riser-downcomer mean temperature difference | 79 °C |
| Buoyancy pumping pressure | 6760 Pa |
| Pressure losses in the spallation region | 2500 Pa |
| Pressure losses in the riser | 700 Pa |
| Pressure losses in the top region | 500 Pa |
| Pressure losses in the heat exchanger | 3000 Pa |
| Pressure losses in the downcomer | 100 Pa |

**Table 5: case d) Natural convection pumping and associated pressure drops**

In order to decrease the pressure drops in the BHE and as a conseguence to increase the LBE mass flow rate a different option for the BHE was considered. In particular a bigger one was chosen (case c),as shown in obtaining higher LBE mass flow rate and better cooling of the window as it is reported in Table 4. With this configuration it was investigated the effects of the variation of the beam power on the natural convection mass flow rate. It can be seen from Figure 11 that the LBE mass

flow rate remain high enough to have a good window cooling even for very small beam power as it is shown in Figure 12.

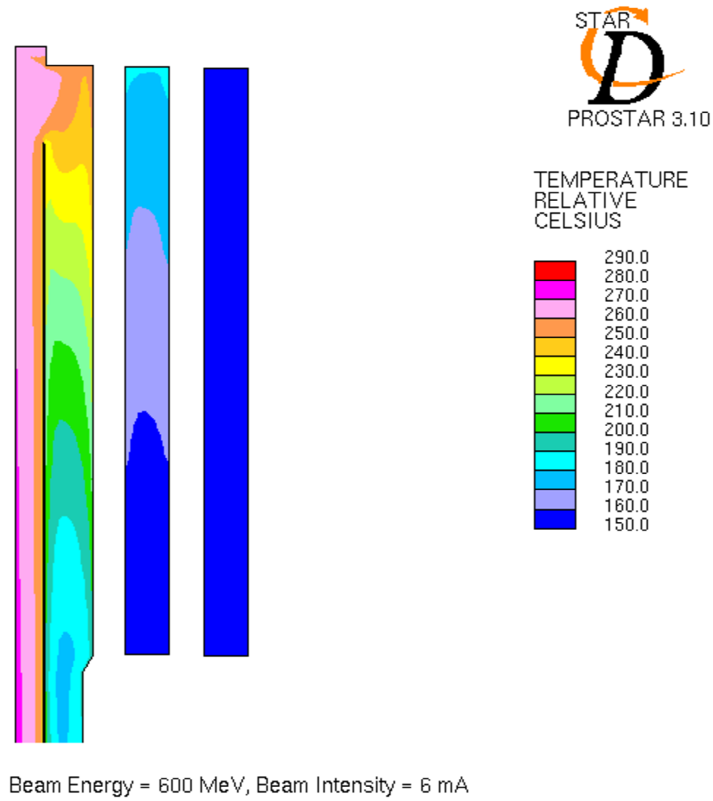


**Figure 10: case c) Temperature distribution in the top zone of the target and in the heat exchanger**

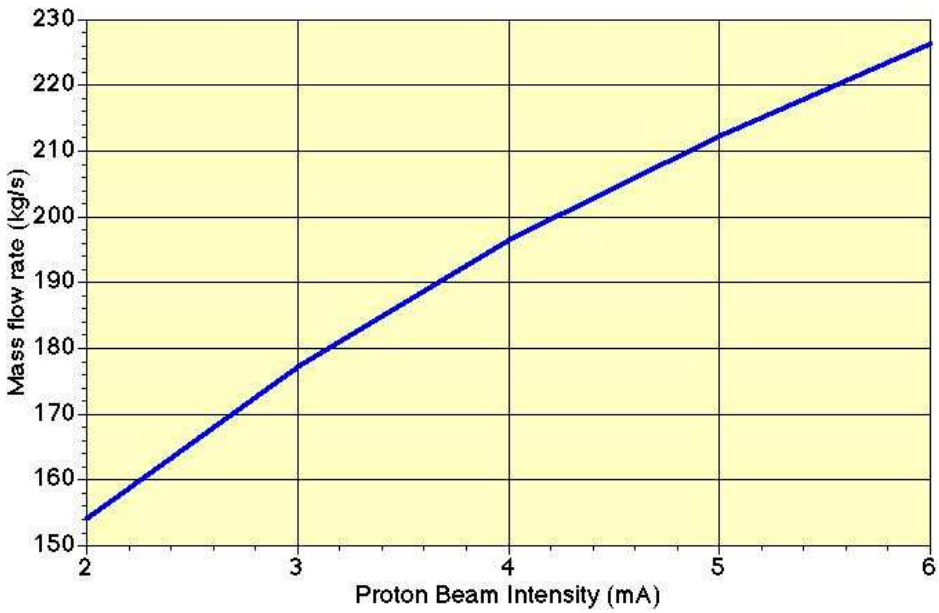


**Figure 11: case c) LBE mass flow rate vs proton beam intensity**

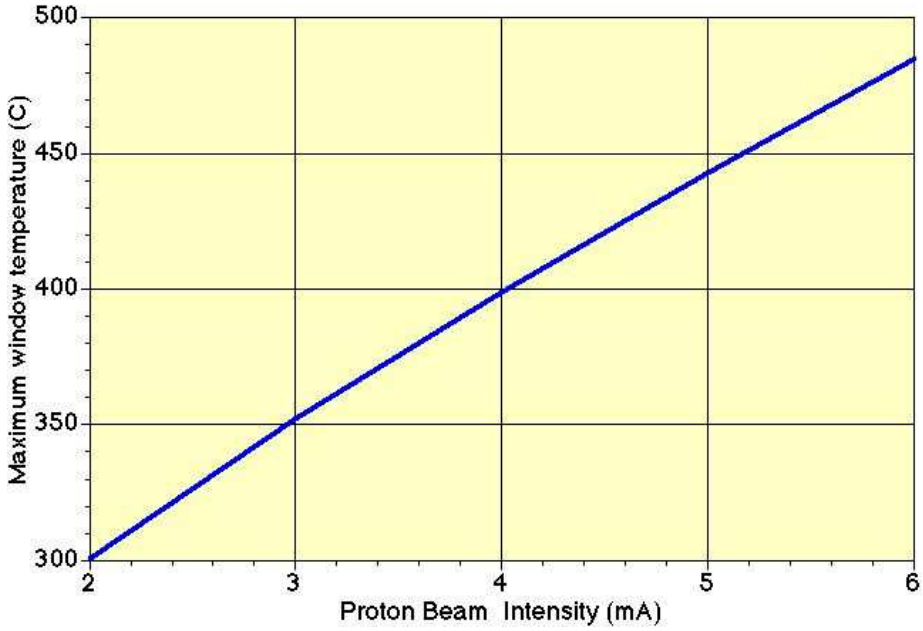


**Figure 12: case c) Maximun window temperature vs proton beam intensity**

Since the more critical part of the whole target device is considered the beam window any trick which can decrese its temperature and as a conseguence related stresses is welcomed. Next case considered (case b) consists in reducing window thickness, so the heat deposition inside the window decrease and it is easier to be removed. Table 4 shows (case b) the main results of simulation which confirm what it was expected. LBE mass flow rate is almost the same and the LBE temperature too. A strong difference can be observed in the window maximum temperature and in particular in the radial gradient of temperature.

| | | | | | |
|---|---|---|---|---|---|
| Energy of proton beam **(input data)** | 600 | 600 | 600 | 600 | MeV |
| Intensity of proton beam **(input data)** | 2 | 2 | 2 | 2 | mA |
| LBE mass flow rate | 155 | 155 | 155 | 155 | kg/s |
| Oil mass flow rate **(input data)** | 31.2 | 31.2 | 31.2 | 31.2 | kg/s |
| Mean LBE temp. in the riser | 302 | 321 | 342 | 362 | °C |
| Mean LBE temp. in the downcomer | 266 | 285 | 306 | 326 | °C |
| Maximum LBE temperature | 378 | 397 | 418 | 438 | °C |
| Minimum window temperature | 340 | 358 | 380 | 399 | °C |
| Maximum window temperature | 385 | 404 | 425 | 445 | °C |
| Max. window temp. radial gradient | 8.2 | 8.2 | 8.1 | 8.1 | °C |
| Mean LBE temp. in the HE inlet | 295 | 314 | 335 | 355 | °C |
| Mean LBE temp. in the HE outlet | 260 | 280 | 300 | 320 | °C |
| Oil temp. in the HE inlet **(input data)** | 250 | 270 | 290 | 310 | °C |
| Oil temp. in the HE outlet | 265 | 285 | 305 | 325 | °C |

**Table 6: HE oil inlet temperature effect at low beam power**

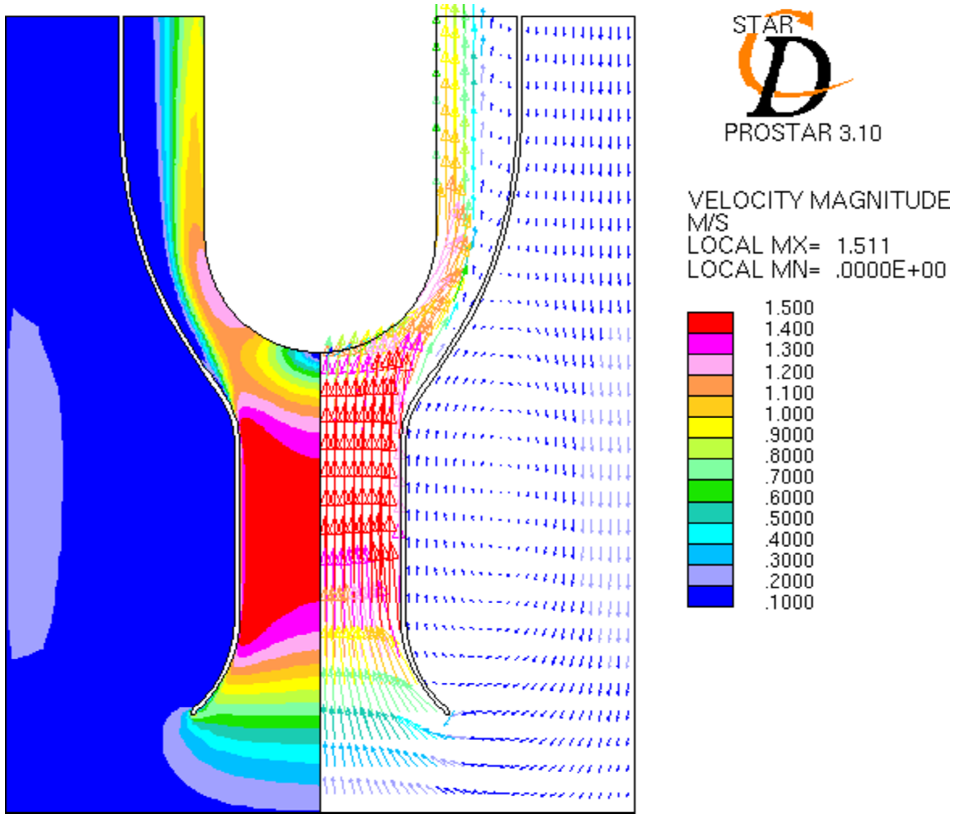


**Figure 13: case a) Velocity field and velocity magnitude distribution in the spallation zone of the target**

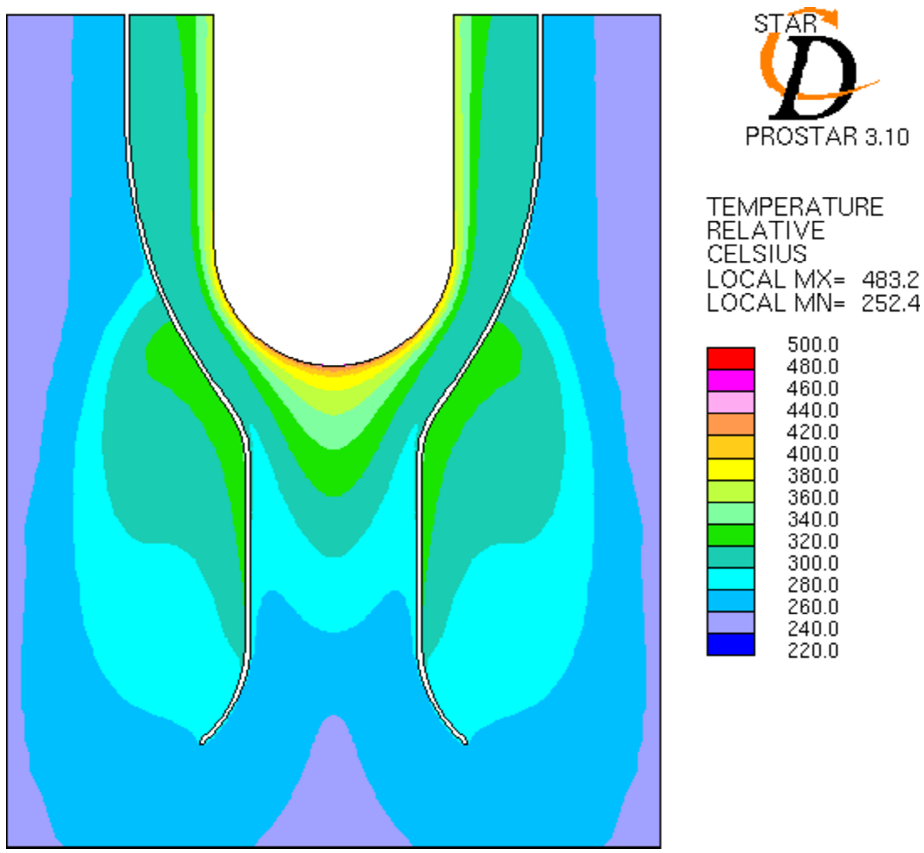


**Figure 14: case a) LBE temperature distribution in the spallation zone of he target**

## Conclusions

## References

**[1]** Energy Amplifier Demonstration Facility Reference Configuration, Summary Report, Ansaldo Nucleare, EA B0.00 1 200, January 1999**.**

**[2]** Star-CD, Version 3.10 manual, Computational Dynamics, London, 1999

**[3]** C. Rubbia et al.,"Conceptual Design for Fast Neutron Operated High Power Energy Amplifier", CERN Report, CERN/AT/95-44 (ET), Geneva, 29th September, 1995.

**[4]** Proceedings of the Meetings ICANS-XIII and ESS-PM4, edited by G. Bauer and R. Bercher, PSI proceedings 95-02, November 1995.

**[5]** Proceedings of the "International Workshop on the Technology and Thermal Hydraulics of Heavy Liquid Metals", compiled by B. R. Appleton and G. S. Bauer, Schruns, Montafon Valley, Austria, March 25-28, 1996.

**[6]** Energy Amplifier Project web page, http://www.crs4.it/~cfdea, CRS4, Centre for Advanced Studies, Research and Development in Sardinia, Cagliari, Italy, 1993-2000

**[7]** Y. Dai, "Martensitic/Ferritic Steels as Container Material for Liquid Mercury Target of ESS", International Workshop on the Technology and Thermal Hydraulic of Heavy Liquid Metals, Schruns, Montafon Valley, Austria, March 25-28, 1996.

**[8]** G. Benamati and I. Ricapito, "Material Selection for the Core of the ADS Demonstrator", ENEA Report, EA D2.02 4401, (1999)

**[9]** A. Fasso' et al., FLUKA 92, Proceedings of the Workshop on Simulating Accelerator Radiation Environments, Santa Fe, 11-15 January 1993.

**[10]** Aragonese, C., Buono, S., Fotia, G., Maciocco, L., Moreau, V. and Sorrentino L., A heat exchanger design for the separated window target of the EADF, CRS4-TECH-REP 00/08.

**[11]** Bellucci, V., Buono, S., Fotia, G., Maciocco, L., Moreau, V., Mulas, M, Siddi, G. and Sorrentino L., Requirements of the beam target of the Energy Amplifier prototype, CRS4-TECH-REP 98/38.

**[12]** Test Specification - Lead-Bismuth Eutectic/Diathermic Oil Interaction, Ansaldo Nucleare, ADS 5 SMEX 0228, November 1999.

**[13]** V. Bellucci, S. Buono, G. Fotia, L. Maciocco, V. Moreau, M. Mulas, G. Siddi, L. Sorrentino, Preliminary sizing of the window-type target of the Energy Amplifier, CRS4-TECH-REP 98/36

**[14]** V. Bellucci, S. Buono, G. Fotia, L. Maciocco, V. Moreau, M. Mulas, G. Siddi, L. Sorrentino, Integration of numerical tools for the combined thermal-hydraulics and structural analysis of Energy Amplifier components, CRS4-TECH-REP 99/14.

**[15]** Perry, R. H. and Don W Green (Eds.), *Perry's Chemical Engineers' Handbook*, sixth edition, Mc Graw Hill, 1984.